Problem Solving Disorders of CSF

2

Tomas Dobrocky and Àlex Rovira

Abstract

Spontaneous Intracranial Hypotension (SIH)

Spontaneous intracranial hypotension (SIH) is a debilitating medical condition, which is perpetuated by the continuous loss of cerebrospinal fluid (CSF) at the level of the spine, and is the top differential diagnosis for patients presenting with orthostatic headache. Neuroimaging plays a crucial role in the diagnostic work-up and monitoring SIH, as it provides objective data in the face of various clinical symptoms and very often a normal opening pressure on lumbar puncture. Brain MRI frequently demonstrates typical signs of CSF depletion and includes homogenous dural enhancement, venous distention, subdural collections, and brain sagging. Three types of CSF leaks may be distinguished: (1) ventral dural leaks due to microspurs, (2) leaking spinal nerve root cysts, (3) or direct CSF venous fistula. The quest for the leak may be the fabled search for the needle in the haystack, scrutinizing the entire spine for a dural breach often the size of pin. The main role of spine imaging is the correct classification and precise localization of CSF leaks. Precise localization of the CSF leak site is crucial to successful treatment, which is generally a targeted percutaneous epidural patch or surgical closure when conservative measures fail to provide long-term relief.

Obstructive Hydrocephalus. Communicating Hydrocephalus. Normal Pressure Hydrocephalus

Modern imaging techniques play an essential role for understanding of the anatomy of the cerebrospinal fluid (CSF) spaces and ventricular system, as well as the hydrodynamics of CSF flow, and consequently in the assessment of the different types of hydrocephalus. Obstructive (non-communicating) hydrocephalus is a complex disorder resulting from an obstruction/blockage of the CSF circulation along one or more of the narrow apertures connecting the ventricles, being the most common type of hydrocephalus in children and young adults. On the other hand, communicating hydrocephalus is defined as a cerebrospinal fluid flow circulation abnormality outside the ventricular system that produces an increase in the ventricular size. Most cases are secondary to obstruction of CSF flow between the basal cisterns and brain convexity and include common conditions such as subarachnoid hemorrhage and meningitis (infectious and neoplastic). In a subset of communicating hydrocephalus, no CSF obstruction can be demonstrated as occurs in normal pressure hydrocephalus (NPH), a complex entity with poorly understood cerebrospinal fluid dynamics. Neuroradiology plays an essential role in the diagnosis of hydrocephalus, and in distinguishing this condition from other causes of ventriculomegaly.

Keywords

Spontaneous intracranial hypotension · SIH · CSF leak · CSF venous fistula · Epidural blood patch · Hydrocephalus · Normal pressure hydrocephalus · Cerebrospinal fluid disorders · Dementia · MRI · CT

T. Dobrocky (✉)
Department of Diagnostic and Interventional Neuroradiology, Bern, Switzerland
e-mail: tomas.dobrocky@insel.ch

À. Rovira
Section of Neuroradiology, Department of Radiology, Hospital Universitari Vall d'Hebron, Barcelona, Spain
e-mail: alex.rovira.idi@gencat.cat

J. Hodler et al. (eds.), *Diseases of the Brain, Head and Neck, Spine 2024-2027*, IDKD Springer Series,
https://doi.org/10.1007/978-3-031-50675-8_2

2.1 Spontaneous Intracranial Hypotension (SIH)

Learning Objectives

- To get acquainted with clinical symptoms, underlying pathomechanism in spontaneous intracranial hypotension (SIH).
- To recognize typical brain imaging findings in SIH and be able to use the Bern SIH score.
- To recognize three spinal CSF leak types and be aware of different myelography techniques.
- To be familiar with treatment options in SIH patients.

Key Points

- Typical brain imaging findings of SIH include dural enhancement, distension of intracranial veins and sinuses, subdural collections, pituitary enlargement, and effacement of subarachnoid cisterns.
- The Bern SIH score is a 9-point, brain MRI-based score, allowing stratification of the likelihood of a spinal CSF leak.
- Low opening pressure on lumbar puncture is not a reliable marker of SIH.
- Non-enhanced MRI of the entire spine, with fat suppression, is important to screen for spinal longitudinal extradural CSF (SLEC) collection and guide further diagnostic steps.
- Spinal CSF leaks do not always occur at the level of prominent disc protrusions or a large nerve root cyst.
- Three types of CSF leaks can be distinguished; (1) ventral dural tears due to an osteogenic microspur, (2) leaking spinal nerve cyst, (3) CSF venous fistula.

According to the International Classification of Headache Disorders (ICHD-3), low opening pressure on lumbar puncture (<6 cm CSF) or classical imaging signs of intracranial hypotension (brain OR spine MRI) is required to fulfill the diagnostic criteria for SIH [1]. Despite the fact that "hypotension" is included in the term "SIH," a low opening pressure on lumbar puncture is only present in about one-third of patient [2, 3]. Consequently, neuroimaging plays a crucial part in the work-up of patients with clinical suspicion of SIH. It is important to distinguish SIH from other pathologies which may be associated with CSF depletion, like post-dural puncture headache (PDPH), rhinorrhea, or CSF loss after surgical interventions, since diagnostic work-up, therapeutic approach, and outcome differ.

2.1.1 Clinical Presentation

The incidence of SIH is 5/100,000 and is almost equal to the incidence of aneurysmatic subarachnoid hemorrhage [4]. Women are twice as often affected than men. The classic clinical hallmark of SIH is orthostatic headache, with an increasing intensity in the upright position and decreases when recumbent. This is most likely due to stretching of pain sensitive fibers in the dura mater, which is more pronounced in the upright position. However, the orthostatic character phenotype may become less apparent in the subacute and chronic stage of the disease, and other non-orthostatic forms including thunderclap, non-positional, exertional, cough related, and "second-half-of-the-day" may occur [5]. Other clinical symptoms include neck pain, tinnitus, changes in hearing, vertigo, nausea, and diplopia. Some of these symptoms are believed to be due to brain sagging which causes stretching of cranial nerves. Other rare presentations of SIH include endocrine disorders due to pituitary enlargement, decreased level of consciousness or coma, which are most likely due to outflow restriction with consecutive thrombosis of the internal cerebral veins [6–8].

2.1.2 Etiology

In total, approximately 100–150 mL of CSF circulates in the intracranial and intraspinal compartments. The CSF encloses the brain parenchyma and spinal cord, providing protection, buoyancy, and a conduit for clearing of metabolic waste products. The CSF is sealed within the confines of the dura while a meticulous balance between production and resorption is maintained. Perturbations of production or resorption disturb this equilibrium and cause symptoms. According to the Monro-Kellie doctrine, the total volume within the confines of the skull is constant and is the sum of the volumes of blood, CSF, and brain parenchyma. Volume loss in one compartment is compensated by a reciprocal volume increase in one or both other compartments. In patients with SIH, the loss of CSF leads predominantly to increased blood volume, which may be appreciated as distension of veins and hyperemia on brain and spine imaging [9, 10].

It is important to note that even though the classical clinical presentation is headache, the underlying cause of the disease is exclusively to be found at the level of the spine. CSF leaks at the level of the skull base are typically not associated with SIH symptoms [11]. Three types of CSF leaks can be distinguished (Table 2.1) [12, 13]. Type I leaks are due to an osteogenic microscope (endplate osteophyte or calcified disc protrusion) penetrating the dura. Type II leaks are due to a leaking spinal nerve cyst. Type III leaks are the

so-called CSF venous fistulas which represent a direct communication between the intrathecal space and the epidural/paraspinal vein [14, 15]. In type I and II leaks, a spinal longitudinal extradural CSF collection (SLEC) is invariably present, thus they may be considered as "wet leaks". On the other hand, type III leaks do not demonstrate a spinal longitudinal extradural CSF collection and thus may be considered "dry leaks".

Table 2.1 Etiology of SIH, brain MRI-based quantitative SIH score (Bern score), typical spine MRI findings

Etiology	Brain MRI imaging	Spine MRI imaging
Type 1: Osteogenic microspur (endplate osteophyte, calcified disc protrusion) Type 2: Leaking nerve root cyst Type 3: CSF venous fistula	Brain SIH score (Bern score) • Major criteria (2 points) 1. Venous distention 2. Pachymeningeal enhancement 3. Suprasellar cistern (≤4 mm) • Minor criteria (1 point) 4. Subdural fluid collection 5. Prepontine cistern (≤5 mm) 6. Mamillopontine distance (≤6.5 mm)	Screen for spinal longitudinal epidural CSF collection (SLEC) SLEC positive ("wet leaks") Type 1 or type 2 leaks SLEC negative ("dry leaks") Type 3 leaks
	Other findings: pituitary enlargement, (infratentorial) superficial siderosis, calvarial hyperostosis	Start with a T2w fat-suppressed MRI Spine MRI has no localizing value for CSF leaks

2.1.3 Diagnostic Work-Up

2.1.3.1 Brain MRI

The diagnostic work-up of SIH patients usually starts with a brain MRI. As proposed by Schievink, the most typical findings include subdural fluid collections, enhancement of the pachymeninges, engorgement of venous structures, pituitary hyperemia, and sagging of the brain (mnemonic: SEEPS) [16] (Fig. 2.1). Additional imaging signs which may be usually be found in long-standing (untreated) SIH include superficial siderosis, calvarial hyperostosis, or enlargement of paranasal sinuses [17, 18].

In 2018, a 9-point, brain MRI-based SIH score (bSIH) allowing stratification of the likelihood of finding a spinal CSF leak in patients with clinically suspected SIH was proposed (Table 2.1) [10]. The score comprises 3 major (2 points each) and 3 minor (1 point each) signs. The major signs are pachymeningeal enhancement, distention of venous sinuses, and effacement of the suprasellar cistern (≤4.0 mm). The minor signs are subdural fluid collection, effacement of the prepontine cistern (≤5.0 mm), and reduced mamillopontine

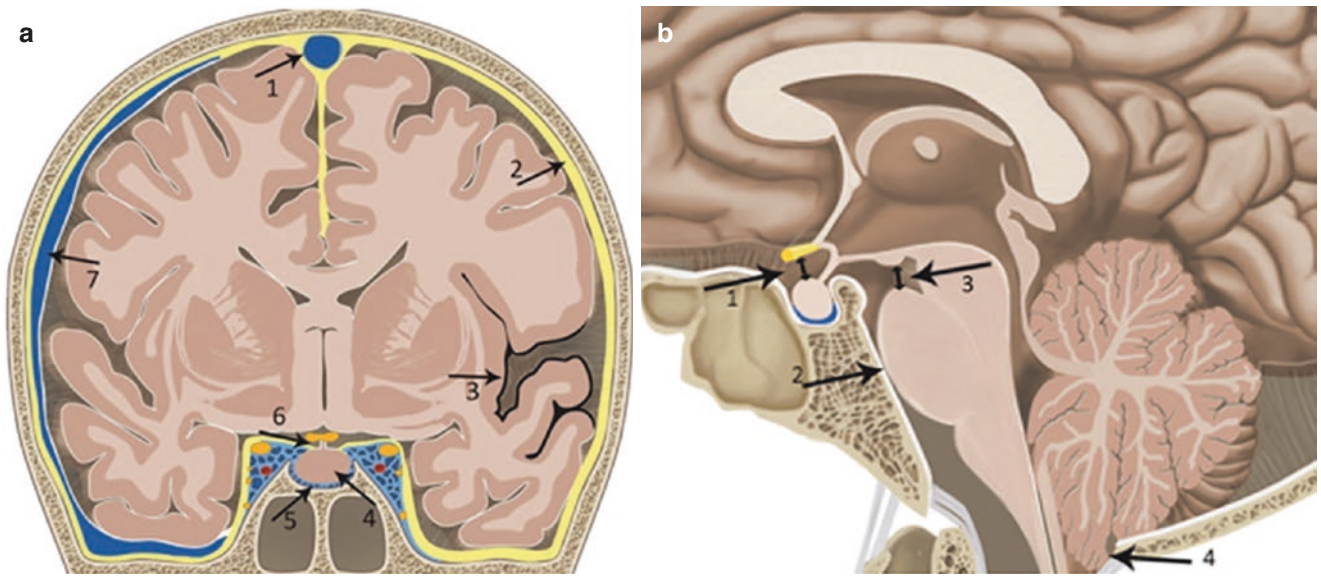

Fig. 2.1 (**a**) Coronal illustration of the brain with typical findings in a patient with a spinal CSF leak with venous distention of the superior sagittal sinus (arrowhead 1), pachymeningeal enhancement (arrowhead 2), superficial siderosis (arrowhead 3), enlarged pituitary (arrowhead 4), prominent intercavernous sinus (arrowhead 5), effaced suprasellar cistern (arrowhead 6), and subdural fluid collection (arrowhead 7). (**b**) Sagittal illustration of the posterior fossa with typical findings in patients with a CSF leak with effaced suprasellar cistern (arrowhead 1; pathologic ≤4 mm), effacement of the prepontine cistern (2; pathologic ≤5 mm), decreased mamillopontine distance (3; pathologic ≤6.5 mm), and low-lying cerebellar tonsils (arrowhead 4). (Reprinted from Dobrocky et al., JAMA 2019)

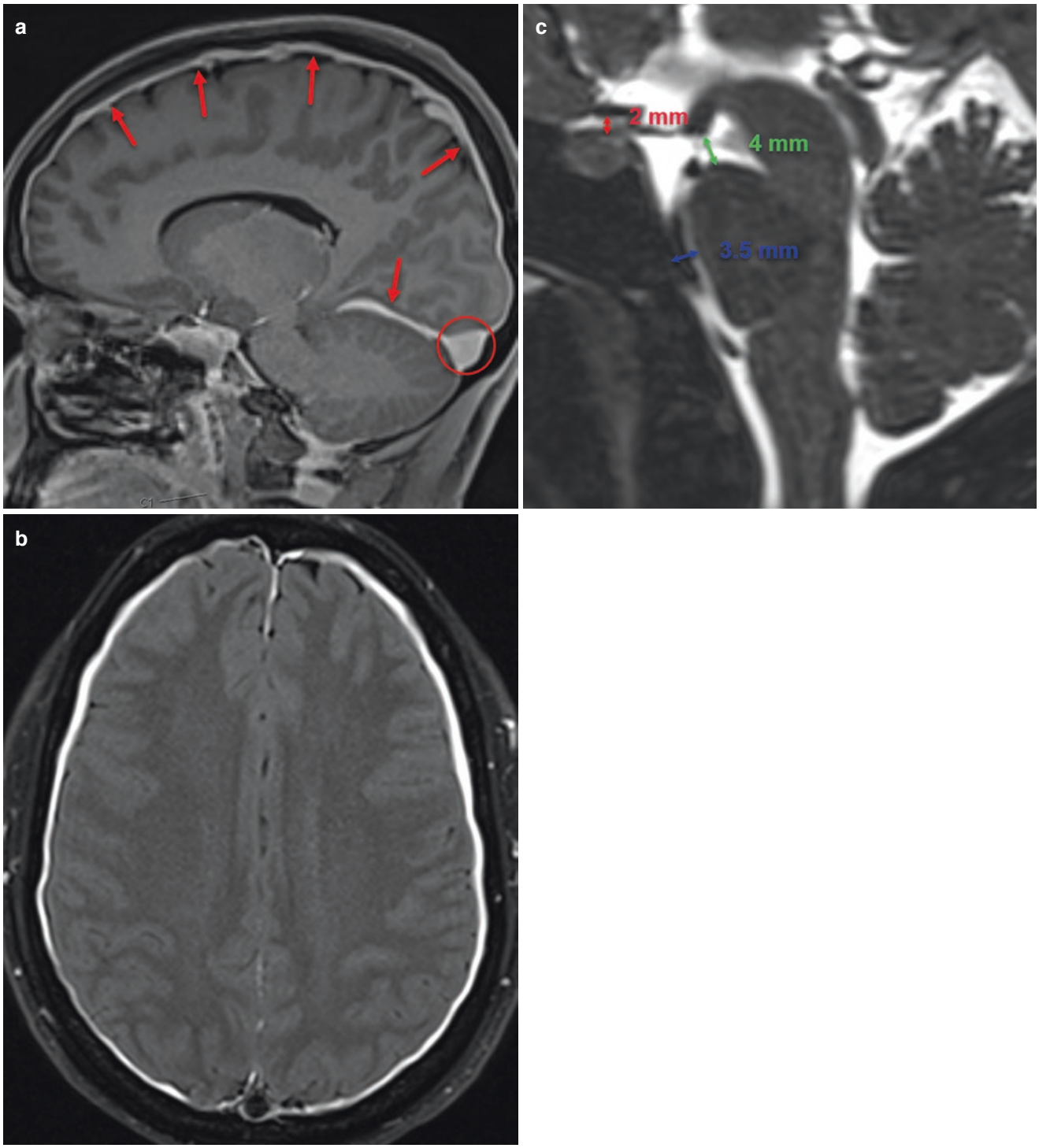

Fig. 2.2 (**a**) Gadolinium-enhanced brain MRI in the sagittal plane demonstrating homogenous and smooth pachymeningeal enhancement and distension of the transverse sinus. (**b**) Flair image in the transversal plane demonstrating bilateral subdural collections. (**c**) T2-weighted MRI in the sagittal plane demonstrating effaced CSF cisterns; suprasellar cistern 2 mm, (pathologic ≤4 mm), prepontine cistern 3.5 mm (pathologic ≤5 mm), mamillopontine distance 4 mm (pathologic ≤6.5 mm)

distance (≤6.5 mm) (Fig. 2.2). Based on the bSIH score ≤2, 3–4, and ≥5, the probability of the myelographic discovery of a CSF leak or CSF venous fistula is low, intermediate, and high, respectively [10, 19].

More recently, the score has been referred to as the Bern SIH score. It has been used as a quantitative tool for therapy monitoring after surgical closure of CSF leaks as well as after endovascular treatment of CSF venous fistulas [20, 21].

2.1.3.2 Spine Imaging

Identification and precise localization of a CSF leak are the main goals of spine imaging. This remains challenging since the quest for the leak may be the fabled search for the needle in the haystack, scrutinizing the entire spine for a dural breach often the size of pin. Various imaging modalities have been used for the spine work-up: unenhanced spine MRI, intrathecal gadolinium-enhanced spine MRI, conventional dynamic myelography, postmyelography CT, dynamic CT myelography, and digital subtraction myelography [22]. Even though a detailed discussion of these techniques is beyond the scope of this chapter, each modality has its unique strengths (spatial/temporal resolution) and shortcomings (intrathecal application of contrast, radiation exposure) which need to be considered.

A non-enhanced MRI of the entire spine should be the first diagnostic step in case of a positive brain MRI or in case of high clinical suspicion of SIH [23]. The spine study should include T2-weighted, fat-suppressed, high-resolution images (Fig. 2.3a) which help to identify any epidural collection of CSF and thus distinguish between "wet leaks" (SLEC +) and "dry leaks" (SLEC −), which guides further diagnostic steps.

In case of intractable SIH, not responding neither to conservative therapy nor to non-targeted epidural blood patch (EBP), the precise localization of a spinal CSF leak is crucial. As previously reported, non-enhanced MRI has no localizing value (accuracy less than 40%) [24]. The reasons for poor accuracy of leak localization on spine MRI are multiple. First, the epidural CSF collection usually spans several vertebral levels and does not allow to pinpoint the culprit lesion at a specific vertebral level [25]. Second, several suspicious culprit lesions are encountered in most patients, including multiple disc protrusions and nerve root cysts. However, in the overwhelming majority of patients, there is only a single site of CSF leakage.

For precise CSF leak localization, three dynamic myelography techniques are available: conventional dynamic myelography (CDM), digital subtraction myelography (DSM), and dynamic CT myelography (DCTM) [26–28]. The practice in different centers may vary according to local availability and expertise. In SLEC positive patients (type 1 and 2), a diagnostic technique with a high temporal resolution is mandatory. Patient positioning should be adapted according to the suspicious findings on spine MRI, prone for suspected ventral osteo-discogenic microspur (type 1 leak) or lateral decubitus for suspected rupture of a spinal nerve root cyst (type 2 leak) [27]. The spinal level where contrast starts to spill from the intrathecal into the epidural compartment when contrast has reached the level of the dural breach needs to be captured during the exam (Fig. 2.3c).

Imaging of CSFVF has evolved over the past few years, and different variations of the technique have been proposed. Lateral decubitus and sustained inspiration during myelography have been reported to increase the diagnostic yield [29, 30]. A CSFVF may be appreciated as an opacified tubular structure ("hyperdense paraspinal vein sign") extending from a nerve root cyst into an epidural or paravertebral vein [15, 31, 32].

2.1.4 Treatment

A three-tier therapeutic model with increasing level of invasiveness for treatment of SIH patients is generally applied, including conservative treatment (bed rest or caffeine), percutaneous treatment with epidural patching (targeted or non-targeted), and surgical or endovascular closure of the CSF leak or fistula.

Conservative measures reported in the literature include bed rest, oral hydration, and oral caffeine administration, however, are unlikely to provide long-term relief in most SIH patients.

When conservative measures fail, non-targeted or targeted image-guided epidural blood patches may be applied. Untargeted epidural blood patch (EBP) is a minimally invasive, readily available, effective symptomatic therapy providing short-term relief in a substantial number of SIH patients. However, according to a recent cohort study, the success rate of permanently sealing a spinal CSF leak is low (<30%), which in turn might explain the high rate of delayed symptom recurrence [33].

Response rates after one EBP reported in the literature range between 36 and 88%. The reason for striking difference in EBP efficacy is manifold. First, the technique varies substantially between studies and depends on the amount (low or high volume), type of injected substance (autologous blood or fibrin), number of injected levels, the way of delivery (targeted vs non-targeted), or the way of application (imaging guided vs blind). Second, several studies do not differentiate between SIH leak type, PDPH, and other possible etiologies of orthostatic headache. Third, the outcome measures are heterogeneous and mainly report short-term improvement in headache severity (<3 months). However, long-term follow-up and objective measures are usually neglected.

Ultimately, in cases of intractable SIH, microsurgical exploration and closure of the dural breach are the treatment of choice [34, 35]. In order to limit the extent of bone removal during surgery, pinpointing the site of dural dehiscence to one vertebral level on dynamic imaging is mandatory for the success of this approach. Recently, Brinjikji et al. proposed a

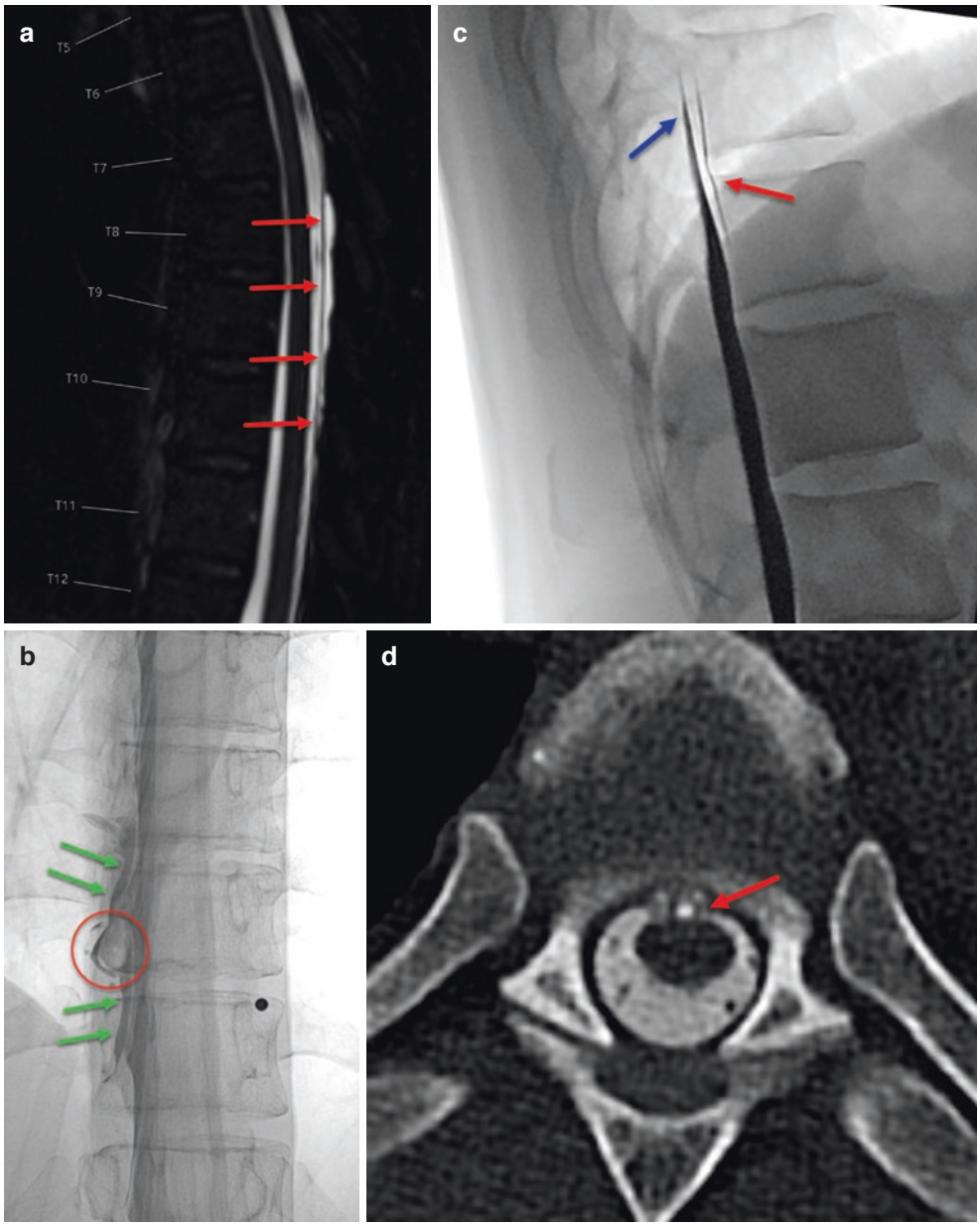

Fig. 2.3 (**a**) T2-weighted, fat-saturated sagittal image demonstrating a CSF collection in the dorsal epidural space - spinal longitudinal epidural CSF collection (SLEC). The posterior dura is clearly visible (red arrows). (**b**) Lateral decubitus myelography demonstrating a type 2 leak with an abnormally enlarged nerve root cyst (red circle) at the level T11 with spilling of intrathecal contrast into the adjacent epidural space (green arrows). (**c**) Conventional dynamic myelography in prone position showing the spill of intrathecal contrast (blue arrow) into the ventral epidural space (red arrow) at T12. (**d**) Postmyelography CT demonstrating a microspur (red arrow) originating at the dorsal endplate and penetrating the dura

transvenous embolization of CSF venous fistulas with very promising results [36].

A recent systematic review on the efficacy of EBP or surgery in SIH patients including 139 studies reported an overall low level of the strength of evidence [37]. In total, 38% studies did not clearly meet the ICHD-3 criteria, CSF leak type was unclear in 78% studies, while nearly all (85%) reported patient symptoms using unvalidated measures. A prospective randomized clinical trial is necessary to clarify the effectiveness of epidural blood patching and surgery in SIH patients.

2.1.5 Concluding Remarks

Due to the growing awareness among headache specialist including, but not limited to, neurologists, neuroradiologists, and neurosurgeons, SIH is increasingly recognized. It typically presents with orthostatic headache and when left untreated may leave the patient psychologically burdened or in despair. Unlike insinuated by the term SIH, true hypotension is an unreliable marker of the disease, underlying on the importance of recognition of objective, however often subtle imaging signs. A meticulous and standardized diagnostic work-up of patients is mandatory in order detect imaging signs of the disease and provide effective therapy.

Take-Home Messages (3–5)

- The **Bern SIH** (bSIH) score is 9-point, brain MRI-based scale that stratifies the likelihood of finding a spinal CSF leak in patients with suspected SIH.
- **Three pathologies** at the level of the spine that may cause SIH: (1) osteogenic microspurs, (2) leaking nerve root cysts, (3) CSF venous fistulas.
- **Non-enhanced MRI** of the entire spine with **fat suppression** is important to screen for spinal longitudinal extradural CSF collection **(SLEC)** and guide further diagnostic steps.
- Spinal CSF leaks do not always occur at the level of prominent disc protrusions; **myelography** with intrathecal contrast and **high temporal resolution** is generally required for leak localization (as opposed to conventional spine MRI).
- **Individualized** treatment approach according to the **leak type** seems warranted (epidural blood patch, microsurgical closure of the leak, transvenous embolization in case of a CSF venous fistula).

2.2 Obstructive Hydrocephalus. Communicating Hydrocephalus. Normal Pressure Hydrocephalus

Learning Objectives

- To gain knowledge on the different types of hydrocephalus.
- To know the MRI protocol required in the diagnostic work-up of suspected hydrocephalus.
- To recognize the typical radiological features of both communicating and non-communicating (obstructive) hydrocephalus.
- To be able to recognize the imaging features that distinguish idiopathic normal pressure hydrocephalus from other causes of ventriculomegaly in the adult population.

Key Points

- Neuroimaging (CT and MRI) allows detailed anatomical and physiological information on hydrocephalus and establishes a classification based on its causal mechanism (non-communicating and communicating).
- High-resolution structural and functional MRI sequences provide the best approach to identify the patency of cerebrospinal flow inside the ventricular system and the cause of hydrocephalus.
- Idiopathic normal pressure hydrocephalus (NPH) is a surgically treatable reversible neurological disorder in which neuroimaging plays an essential role in its diagnosis and in predicting surgical response.

2.2.1 Hydrocephalus

Hydrocephalus is currently defined as ventricular dilatation associated with a decrease in extraventricular subarachnoid spaces. The degree of ventricular dilation and the damage produced to brain tissue will depend on various factors, such as the cause and speed of onset of hydrocephalus, and the age of the patient.

With the advent, first of CT and later of MRI, it has been possible to obtain detailed anatomical and physiological information on hydrocephalus and to establish a classification based on its causal mechanism (non-communicating and communicating), a fact that has obvious therapeutic implications (Table 2.2).

Usually brain CT is the first-line imaging procedure, especially in emergency cases with acute hydrocephalus. However, MRI is the method of choice in detailed assessment of this condition. Contrast media injection is not required for the diagnosis unless there is a suspicion of a neoplastic or an inflammatory process. The main purpose of the diagnostic procedures in patient with obstructive hydrocephalus is to find a lesion impeding the cerebrospinal fluid (CSF) flow within the ventricular system and to differentiate this condition from communicating hydrocephalus and other non-hydrocephalic cause of ventricular enlargement such as brain atrophy [38, 39].

In addition to conventional structural MRI sequences, other dedicated sequences should be considered in the assessment of hydrocephalus [40, 41]. Cardiac-gated phase contrast MRI (PC-MRI) is extremely sensitive to CSF flow and has demonstrated value in demonstrating patency of intraventricular CSF circulation (particularly aqueduct patency), but does not offer anatomical information of CSF pathways. Combination of heavily 3D T2-weighted sequences such as CISS (constructive interference steady state) or FIESTA (Fast Imaging Employing Steady-State Acquisition) that offer superb anatomical information, and 3D T2-weighted turbo/fast spin-echo sequences such as SPACE (sampling perfection with application optimized contrast using different flip angle evolutions), VISTA (volume isotropic turbo spin echo **a**cquisition), or CUBE that are

Table 2.2 Causes of hydrocephalus

Non-communicating (obstructive)	Communicating
Any obstacle compressing the foramina from the outside or any intraventricular obstructive lesion at the level of: 1. **Foramen of Monro**: Colloid cyst, tumors (ependymoma, subependymomas, central neurocytoma, glial tumors), adhesions 2. **Cerebral aqueduct**: • Non-neoplastic intrinsic lesions (idiopathic/congenital/inflammatory): webs/adhesions/forking, cysts • Periaqueductal lesions: pineal gland tumors, tectum glioma, tentorial meningioma, metastasis, infection (meningitis/ventriculitis, abscess), cerebral vascular malformation (vein of Galen aneurysm) • Giant cystic mesencephalic Virchow-Robin spaces 3. **Trapped fourth ventricle** (obstruction of all CSF pathways of the fourth ventricle, including foramina of Luschka and Magendie, as well as aqueduct): previous ventricular shunting for hydrocephalus, infection, intraventricular hemorrhage, and post-inflammatory changes after posterior fossa surgery 4. **Fourth ventricular outlets**: cerebellar infarct, posterior fossa tumors (metastasis, meningioma, astrocytoma, medulloblastomas), hemorrhage, meningitis, Dandy–Walker malformation 5. **Foramen magnum:** metabolic diseases, developmental abnormalities, Chiari malformations, osteochondrodysplasia	**With obstruction of CSF absorption**: • Subarachnoid hemorrhage • Meningitis—bacterial, aseptic • Leptomeningeal carcinomatosis • Vestibular schwannoma **Without obstruction of CSF absorption: normal pressure hydrocephalus (NPH)** • Secondary (sNPH): subarachnoid hemorrhage, meningitis • Idiopathic (iNPH)

Table 2.3 Protocol recommendations for MRI in suspected hydrocephalus of unknown origin

• 2D/3D sagittal unenhanced T1-weighted (with multiplanar reconstruction)
• 2D axial T2-weighted
• 2D transverse/3D sagittal T2-FLAIR
• 3D sagittal CISS/FIESTA
• 3D sagittal T2-weighted SPACE/VISTA/CUBE
• 2D/3D susceptibility-based sequences
If infectious meningitis or leptomeningeal metastasis suspected add:
• 2D transverse/3D sagittal contrast-enhanced T2-FLAIR
• 2D transverse-coronal/3D sagittal contrast-enhanced T1-weighted

highly sensitive to CSF flow, provides an easy evaluation of CSF pathway and circulation to establish the patency of CSF flow [41]. It has been shown that these sequences provide adequate morphological and similar functional information of CSF patency to cine PC-MRI [42] and should be considered within the imaging strategy for assessing CSF circulation patency in clinical practice (Table 2.3; Fig. 2.4).

2.2.2 Radiological Findings

The typical radiological findings which raise the suspicion of any form of hydrocephalus are as follows:

1. Enlargement of the ventricles that can be quantified by using the Evans' index. The Evans' index is the ratio of maximum width of the frontal horns of the lateral ventricles and maximum internal diameter of skull at the same level measured in axial CT and MRI images. A value of >0.3 is considered abnormal.
2. Dilatation of temporal horns—a very sensitive sign of hydrocephalus. Temporal ventricular horns dilate first due to relatively little resistance of choroidal fissure to expansion and relative bulk of basal ganglia "tamponading" lateral ventricles.
3. Dilatation of the third ventricular recesses.
4. Reduced mamillopontine distance.
5. Upward bowing and thinning of the corpus callosum.
6. Disproportionately narrowed cortical sulci, although they may be normal especially if there was pre-existing widening.

Acute hydrocephalus is an emergency condition requiring urgent treatment because it may lead to severe complications such as cerebral infarction, persistent blindness, herniation, or even death. The most important findings on MRI which enable differentiation between acute and chronic hydrocephalus are hyperintense bands in the periventricular white matter found on T2-weighted or T2-FLAIR images which are compatible with acute interstitial oedema, referred to as transependymal oedema or diapedesis (Fig. 2.5). On CT, these areas appear as low-density regions around the margins of the ventricles.

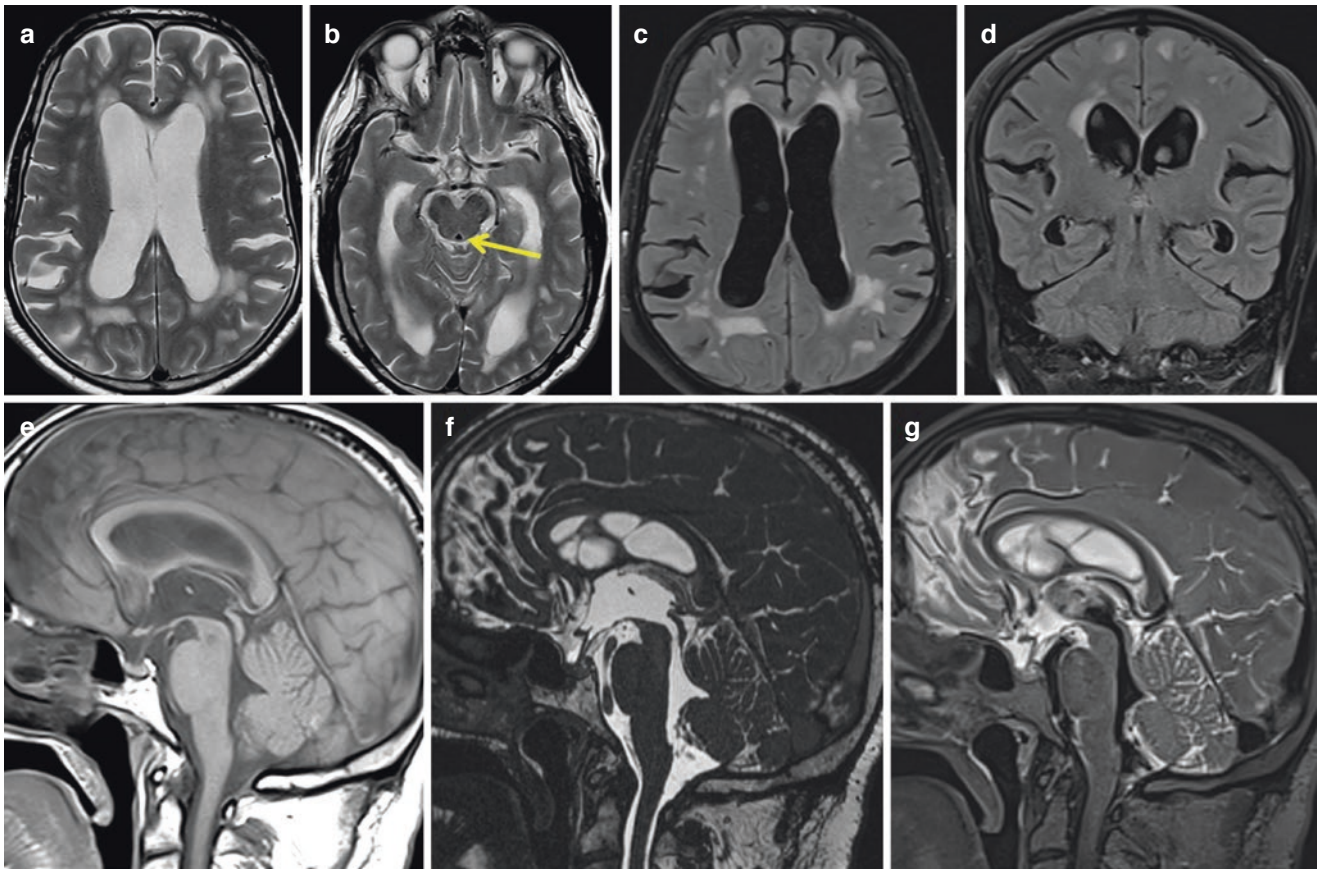

Fig. 2.4 Brain MRI recommended protocol in the diagnostic work-up of hydrocephalus. Axial T2-weighted images (**a**, **b**) show ventriculomegaly associated with the presence of flow void inside the aqueduct (arrow). Transverse and coronal T2-FLAIR images (**c**, **d**) shows mild enlargement of Sylvian fissures associated with blockage of upper convexity CSF spaces. Midsagittal T1-weighted (**e**), 3D CISS (**f**), and 3D SPACE (**g**) images shows a morphological normal aqueduct with marker flow void. These findings indicated the diagnosis of normal pressure hydrocephalus

2.2.3 Non-communicating (Obstructive) Hydrocephalus

Obstructive (non-communicating) hydrocephalus is a complex disorder resulting from an obstruction/blockage of the cerebrospinal fluid circulation along one or more of the narrow apertures connecting the ventricles [40]. This type of hydrocephalus is caused by a variety of conditions including the typical obstruction sites at the level of foramen of Monro, cerebral aqueduct (Fig. 2.6), fourth ventricular outlets (Fig. 2.7), and foramen magnum, produced by either any lesion in the form of space-occupying lesion compressing the foramina from the outside, or any intraventricular obstructive lesion including tumour or haemorrhage [43, 44] (Table 2.2).

Since obstructive hydrocephalus may be a life-threatening condition, this condition requires a prompt and accurate diagnosis in order to offer the most adequate treatment.

2.2.4 Communicating Hydrocephalus

Communicating hydrocephalus is defined as a CSF flow circulation abnormality outside the ventricular system that produces an increase in the ventricular size. Most cases are secondary to obstruction of CSF flow between the basal cisterns and brain convexity and include common conditions such as subarachnoid hemorrhage (SAS), bacterial and aseptic meningitis, and leptomeningeal carcinomatosis. Based on this concept, communicating hydrocephalus is usually associated with CSF absorption impairment, and for that reason this type of hydrocephalus could be better classified as communicating with obstruction, to differentiate them from normal pressure hydrocephalus (NPH), in which there is no objective obstruction of CSF circulation and absorption [45, 46]. Important radiological features that distinguish this type of hydrocephalus from other causes of ventriculomegaly are dilatation of the temporal horns; ballooning of the third ventricular walls, including its anterior recesses; upward bowing

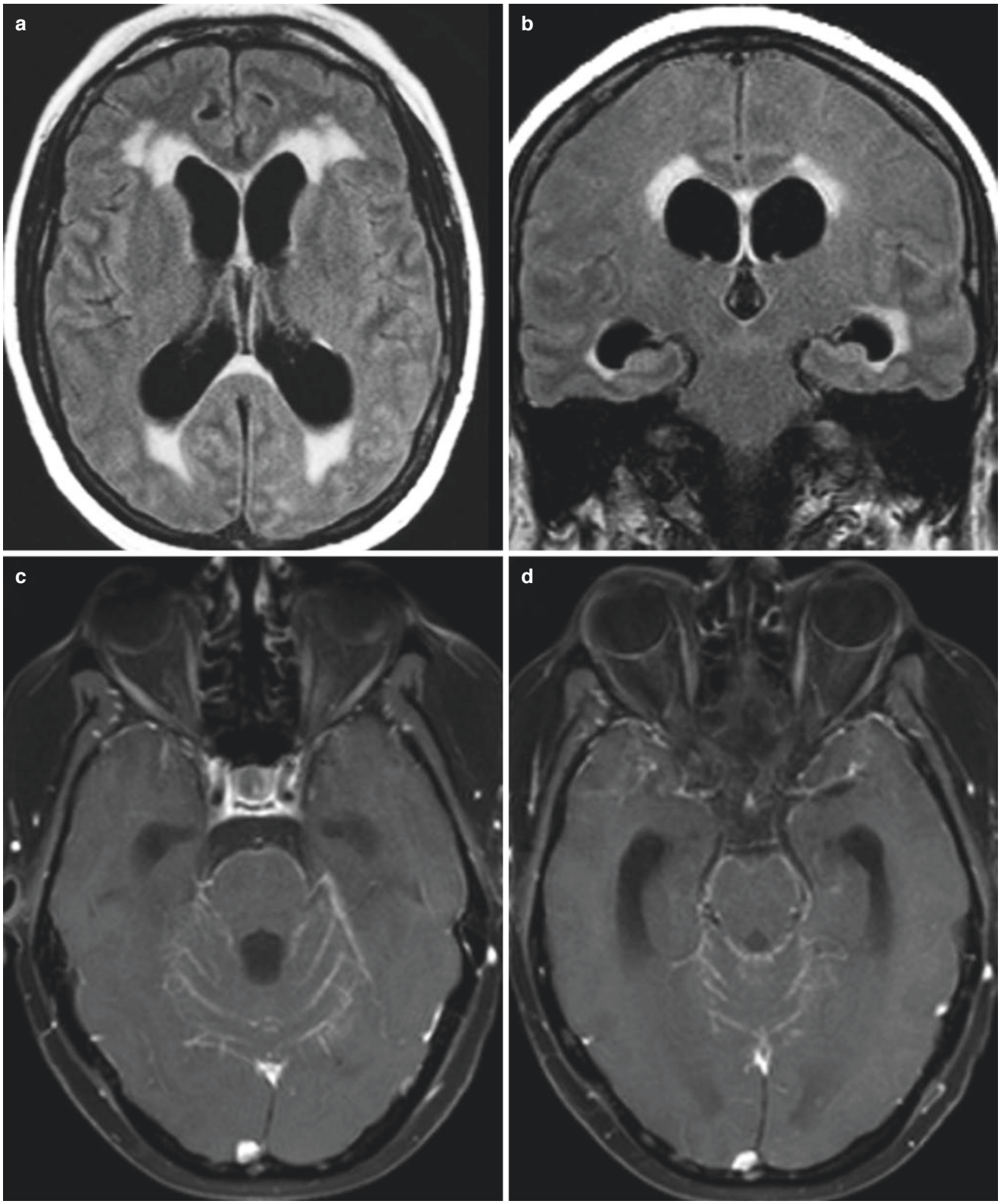

Fig. 2.5 Acute communicating hydrocephalus secondary to leptomeningeal carcinomatosis in a patient previously diagnosis of breast cancer. Transverse (**a**) and coronal (**b**) T2-FLAIR images and contrast-enhanced T1-weighted images (**c**, **d**). Observe the ventriculomegaly associated with periventricular interstitial edema and diffuse leptomeningeal enhancement surrounding the brain stem and cerebellum

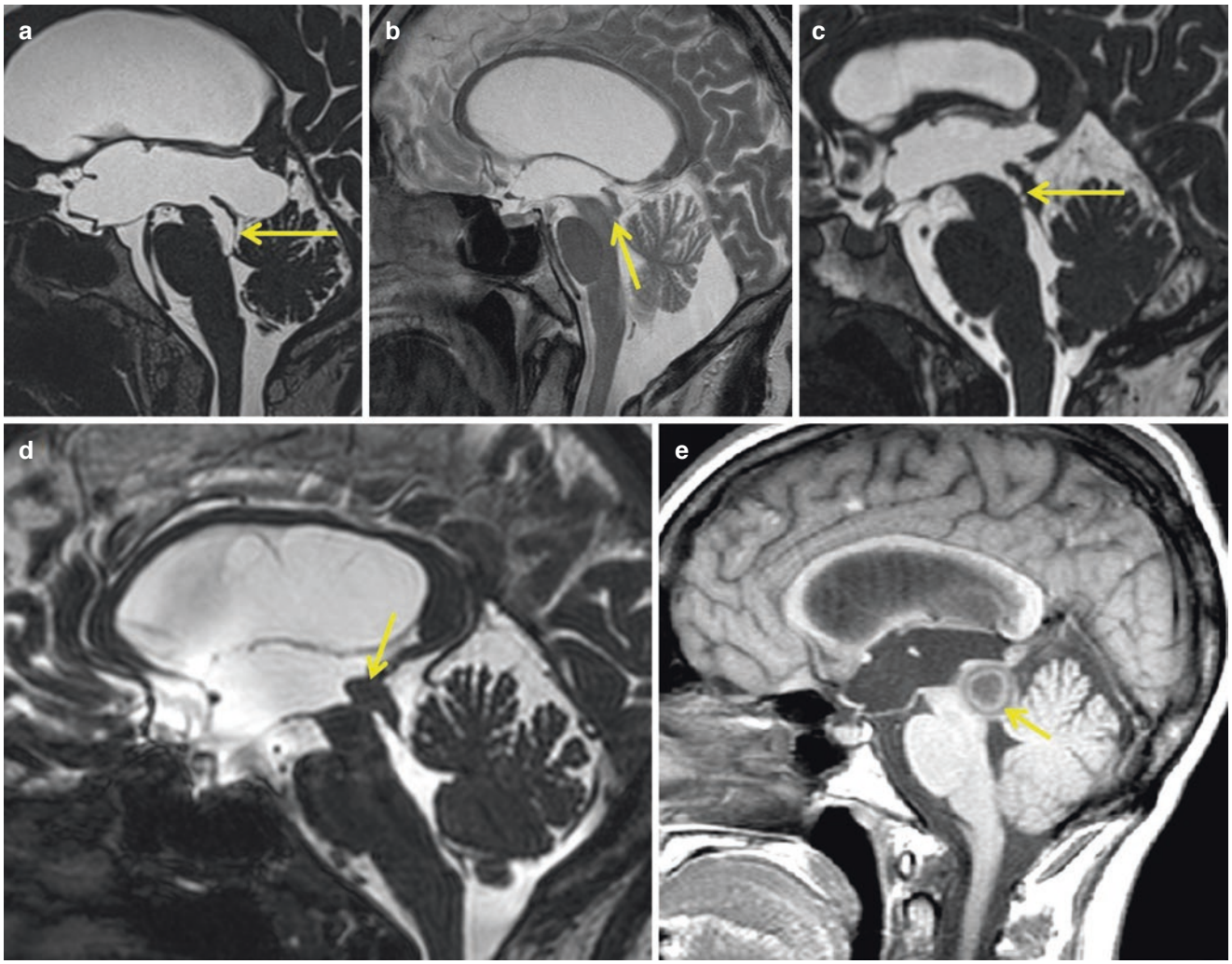

Fig. 2.6 Examples of non-tumoral and tumoral aqueductal stenosis detected on midsagittal MR images. (**a**) Web; (**b**) Adhesion; (**c**) Forking; (**d**) Tectal glioma; (**e**) Abscess

of the corpus callosum; and demonstration of CSF circulation patency inside the ventricular system (Fig. 2.4).

Normal pressure hydrocephalus (NPH) is characterized by the triad of gait disturbance, mental deterioration, and urinary incontinence, which are associated with enlargement of the ventricular system and normal CSF pressure. About 50% of cases with NPH have a known cause (secondary or symptomatic NPH [sNPH]), such as meningitis, subarachnoid haemorrhage, or cranial trauma, while the remaining 50% of cases are idiopathic (iNPH), usually presenting in the seventh decade of life. Typical structural brain changes in iNPH have been grouped under the term "disproportionately enlarged subarachnoid space hydrocephalus" (DESH), which refers to the combination of 1/ventriculomegaly (Evans index >0.3); 2/narrow high-convexity and medial subarachnoid spaces; and 3/Enlarged Sylvian fissures (disproportionate distribution of the CSF between the inferior and superior subarachnoid spaces). Shinoda et al. [47] have proposed the incorporation of two additional radiological features (callosal angle and focal sulcal dilation) [48, 49] to these three components, which in combination have a high positive predictive value in relation to neurological improvement after surgery (Fig. 2.8). Not every patient with possible or probable iNPH will be a candidate for shunt surgery, and the risk to benefit ratio has to be assessed on individual bases. Diagnostic test used for selecting patients for shunt surgery includes those based on surgical invasive procedures (CSF dynamics and intracranial pressure monitoring) [50, 51], and those based on morphological or functional MRI studies [52, 53].

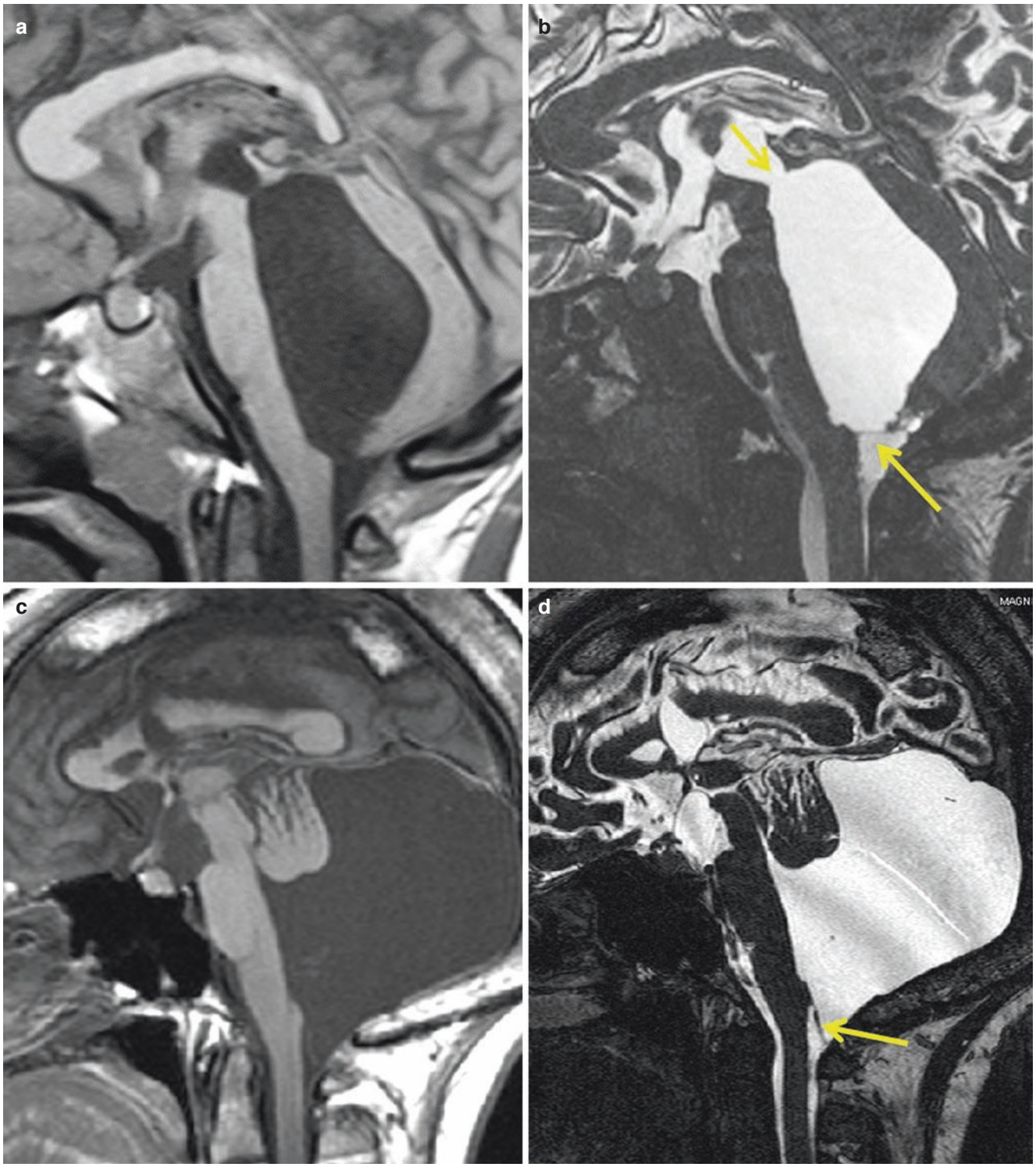

Fig. 2.7 Fourth ventricle hydrocephalus. Non-communicating hydrocephalus secondary to inflammatory obstruction of the fourth ventricle outlets (trapped fourth ventricle) in patients with history of perinatal infection. Sagittal T1-weighted (**a**) shows marked isolated fourth ventricle enlargement. The high-resolution 3D CISS images (**b**) shows thin bands that blocked the CSF pathways of the fourth ventricle, including foramen of Magendie, and aqueduct (arrows). Non-communicating hydrocephalus secondary to obstruction of the fourth ventricle outlets in Dandy–Walker malformation. Sagittal T1-weighted (**c**) shows hypoplasia of the cerebellar vermis and cephalad rotation of the vermian remnant, cystic dilatation of the fourth ventricle extending posteriorly and enlarged posterior fossa. The high-resolution 3D CISS images (**d**) shows a thin band that blocked the foramina of Magendie (arrow)

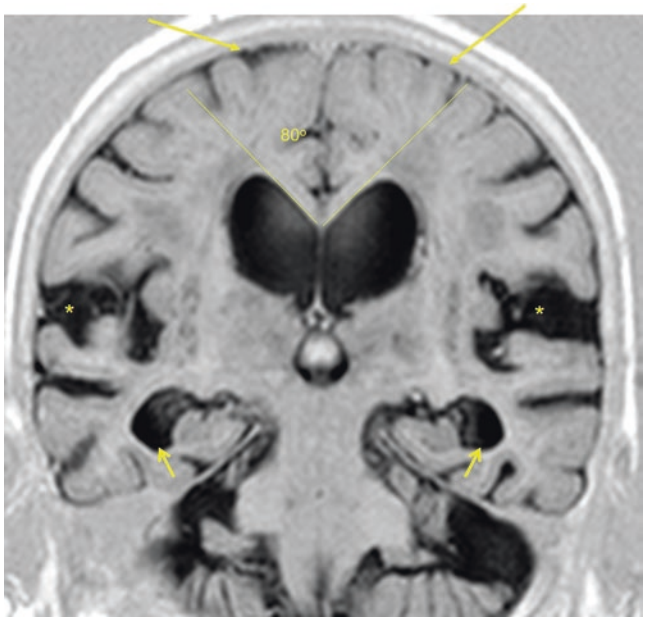

Fig. 2.8 73-year-old man with a diagnosis of idiopathic normal pressure hydrocephalus. All components of DESH are clearly visible on this coronal T1-weighted image. Ventriculomegaly (Evans index >0.3); high-convexity tightness (arrows); enlarged Sylvian fissures (asterisks); reduced callosal angle; and marked dilatation of both temporal horns not explained by hippocampal atrophy (arrows)

2.2.5 Concluding Remarks

Structural and functional MRI play an essential role for understanding the anatomy of the CSF spaces and ventricular system, as well as the hydrodynamics of CSF flow. These principles are important to the comprehension of the different types of hydrocephalus. Combination of heavily 3D T2-weighted sequences such as CISS or FIESTA that offer superb anatomical information, and 3D T2-weighted turbo/fast spin-echo sequences such as SPACE, VISTA, or CUBE that are highly sensitive to CSF flow, provides an easy evaluation of CSF pathway and circulation, and allows an accurate distinction between non-communicating from communicating hydrocephalus and identification of the causative mechanism of these two types of hydrocephalus.

Take-Home Messages (3–5)

- MRI is the imaging modality of choice in the diagnosis and management of hydrocephalus.
- Conventional MRI sequences associated with high-resolution 3D T2-weighted sequences seem to be most efficient MRI strategy for assessing CSF pathways and circulation, and consequently in the identification of the causative mechanism of both communicating and non-communicating hydrocephalus.
- Presence of disproportionately enlarged subarachnoid spaces (DESH) is a useful MRI feature for establishing the diagnosis of idiopathic normal pressure hydrocephalus.

References

1. Vincent M, Wang SJ. Headache Classification Committee of the International Headache Society (IHS) The International Classification of Headache Disorders. Cephalalgia. 2018;38(1):1–211. https://doi.org/10.1177/0333102417738202.
2. Kranz PG, Tanpitukpongse TP, Choudhury KR, Amrhein TJ, Gray L. How common is normal cerebrospinal fluid pressure in spontaneous intracranial hypotension? Cephalalgia. 2016;36(13):1209–17. http://www.ncbi.nlm.nih.gov/pubmed/26682575.
3. Häni L, Fung C, Jesse CM, Ulrich CT, Miesbach T, Cipriani DR, et al. Insights into the natural history of spontaneous intracranial hypotension from infusion testing. Neurology. 2020;95(3):e247–55. http://www.ncbi.nlm.nih.gov/pubmed/32522800.
4. Schievink WI, Maya MM, Moser F, Tourje J, Torbati S. Frequency of spontaneous intracranial hypotension in the emergency department. J Headache Pain. 2007;8(6):325–8.
5. Mokri B, Aksamit A, Atkinson J. Paradoxical postural headaches in cerebrospinal fluid leaks. Cephalalgia. 2004;24(10):883–7. https://doi.org/10.1111/j.1468-2982.2004.00763.x.
6. Yamamoto M, Suehiro T, Nakata H, Nishioka T, Itoh H, Nakamura T, et al. Primary low cerebrospinal fluid pressure syndrome associated with galactorrhea. Intern Med. 1993;32(3):228–31. http://www.ncbi.nlm.nih.gov/pubmed/8329818.
7. Arai S, Takai K, Taniguchi M. The algorithm for diagnosis and management of intracranial hypotension with coma: report of two cases. Surg Neurol Int. 2020;11(267):2–4.
8. Takai K, Niimura M, Hongo H, Umekawa M, Teranishi A, Kayahara T, et al. Disturbed consciousness and coma: diagnosis and management of intracranial hypotension caused by a spinal cerebrospinal fluid leak. World Neurosurg. 2019;121:e700–11. https://linkinghub.elsevier.com/retrieve/pii/S1878875018322484.
9. Kranz PG, Tanpitukpongse TP, Choudhury KR, Amrhein TJ, Gray L. Imaging signs in spontaneous intracranial hypotension: prevalence and relationship to CSF pressure. Am J Neuroradiol. 2016;37(7):1374–8.
10. Dobrocky T, Grunder L, Breiding PS, Branca M, Limacher A, Mosimann PJ, et al. Assessing spinal cerebrospinal fluid leaks in spontaneous intracranial hypotension with a scoring system based on brain magnetic resonance imaging findings. JAMA Neurol. 2019;18:1–8.
11. Schievink WI, Schwartz MS, Maya MM, Moser FG, Rozen TD. Lack of causal association between spontaneous intracranial hypotension and cranial cerebrospinal fluid leaks. J Neurosurg. 2012;116(4):749–54. http://www.ncbi.nlm.nih.gov/pubmed/22264184.
12. Farb RI, Nicholson PJ, Peng PW, Massicotte EM, Lay C, Krings T, et al. Spontaneous intracranial hypotension: a systematic imaging approach for CSF leak localization and management based on MRI and digital subtraction myelography. AJNR Am J Neuroradiol. 2019;40(4):745–53. http://www.ncbi.nlm.nih.gov/pubmed/30923083.

13. Schievink WI, Maya MM, Jean-Pierre S, Nuño M, Prasad RS, Moser FG. A classification system of spontaneous spinal CSF leaks. Neurology. 2016;87(7):673–9. http://www.ncbi.nlm.nih.gov/pubmed/27440149.
14. Kumar N, Diehn FE, Carr CM, Verdoorn JT, Garza I, Luetmer PH, et al. Spinal CSF venous fistula: a treatable etiology for CSF leaks in craniospinal hypovolemia. Neurology. 2016;86(24):2310–2. http://www.ncbi.nlm.nih.gov/pubmed/27178701.
15. Schievink WI, Moser FG, Maya MM. CSF-venous fistula in spontaneous intracranial hypotension. Neurology. 2014;83(5):472–3. http://www.ncbi.nlm.nih.gov/pubmed/24951475.
16. Schievink WI. Spontaneous spinal cerebrospinal fluid and ongoing investigations in this area. JAMA. 2006;295(19):2286–96.
17. Schievink WI, Maya MM. Spinal meningeal diverticula, spontaneous intracranial hypotension, and superficial siderosis. Neurology. 2017;88(9):916–7. http://www.ncbi.nlm.nih.gov/pubmed/28130464.
18. Johnson DR, Carr CM, Luetmer PH, Diehn FE, Lehman VT, Cutsforth-Gregory JK, et al. Diffuse calvarial hyperostosis in patients with spontaneous intracranial hypotension. World Neurosurg. 2021;146:e848–53.
19. Kim DK, Carr CM, Benson JC, Diehn FE, Lehman VT, Liebo GB, et al. Diagnostic yield of lateral decubitus digital subtraction myelogram stratified by brain MRI findings. Neurology. 2021;96(9):e1312–8. https://doi.org/10.1212/WNL.0000000000011522.
20. Brinjikji W, Garza I, Whealy M, Kissoon N, Atkinson JLD, Savastano L, et al. Clinical and imaging outcomes of cerebrospinal fluid-venous fistula embolization. J Neurointerv Surg. 2022;14(10):953–6.
21. Dobrocky T, Häni L, Rohner R, Branca M, Mordasini P, Pilgram-Pastor S, et al. Brain spontaneous intracranial hypotension score for treatment monitoring after surgical closure of the underlying spinal dural leak. Clin Neuroradiol. 2022;32(1):231–8.
22. Kranz PG, Luetmer PH, Diehn FE, Amrhein TJ, Tanpitukpongse TP, Gray L. Myelographic techniques for the detection of spinal CSF leaks in spontaneous intracranial hypotension. AJR Am J Roentgenol. 2016;206(1):8–19. http://www.ncbi.nlm.nih.gov/pubmed/26700332.
23. Watanabe A, Horikoshi T, Uchida M, Koizumi H, Yagishita T, Kinouchi H. Diagnostic value of spinal MR imaging in spontaneous intracranial hypotension syndrome. Am J Neuroradiol. 2009;30(1):147–51.
24. Dobrocky T, Winklehner A, Breiding PS, Grunder L, Peschi G, Häni L, et al. Spine MRI in spontaneous intracranial hypotension for CSF leak detection: nonsuperiority of intrathecal gadolinium to heavily T2-weighted fat-saturated sequences. AJNR Am J Neuroradiol. 2020;41(7):1309–15. https://doi.org/10.3174/ajnr.A6592.
25. Schievink WI, Maya MM, Chu RM, Moser FG. False localizing sign of cervico-thoracic CSF leak in spontaneous intracranial hypotension. Neurology. 2015;84(24):2445–8.
26. Schievink WI, Maya MM, Moser FG, Prasad RS, Cruz RB, Nuño M, et al. Lateral decubitus digital subtraction myelography to identify spinal CSF-venous fistulas in spontaneous intracranial hypotension. J Neurosurg Spine. 2019;31(1):902–5. http://www.ncbi.nlm.nih.gov/pubmed/31518974.
27. Piechowiak EI, Pospieszny K, Haeni L, Jesse CM, Peschi G, Mosimann PJ, et al. Role of conventional dynamic myelography for detection of high-flow cerebrospinal fluid leaks: optimizing the technique. Clin Neuroradiol. 2020;31:633–41. https://doi.org/10.1007/s00062-020-00943-w.
28. Dobrocky T, Mosimann PJ, Zibold F, Mordasini P, Raabe A, Ulrich CT, et al. Cryptogenic cerebrospinal fluid leaks in spontaneous intracranial hypotension: role of dynamic CT myelography. Radiology. 2018;289(3):766–72. http://www.ncbi.nlm.nih.gov/pubmed/30226459.
29. Kim DK, Brinjikji W, Morris PP, Diehn FE, Lehman VT, Liebo GB, et al. Lateral decubitus digital subtraction myelography: tips, tricks, and pitfalls. AJNR Am J Neuroradiol. 2020;41(1):21–8. http://www.ncbi.nlm.nih.gov/pubmed/31857327.
30. Amrhein TJ, Gray L, Malinzak MD, Kranz PG. Respiratory phase affects the conspicuity of CSF-venous fistulas in spontaneous intracranial hypotension. AJNR Am J Neuroradiol. 2020;41(9):1754–6. http://www.ncbi.nlm.nih.gov/pubmed/32675336.
31. Clark MS, Diehn FE, Verdoorn JT, Lehman VT, Liebo GB, Morris JM, et al. Prevalence of hyperdense paraspinal vein sign in patients with spontaneous intracranial hypotension without dural CSF leak on standard CT myelography. Diagn Interv Radiol. 2018;24(1):54–9.
32. Kranz PG, Amrhein TJ, Gray L. CSF venous fistulas in spontaneous intracranial hypotension: imaging characteristics on dynamic and CT myelography. Am J Roentgenol. 2017;209(6):1360–6.
33. Piechowiak EI, Aeschimann B, Häni L, Kaesmacher J, Mordasini P, Jesse CM, et al. Epidural blood patching in spontaneous intracranial hypotension-do we really seal the leak? Clin Neuroradiol. 2023;33(1):211–8.
34. Schievink WI, Morreale VM, Atkinson JLD, Meyer FB, Piepgras DG, Ebersold MJ. Surgical treatment of spontaneous spinal cerebrospinal fluid leaks. J Neurosurg. 1998;88(2):243–6. https://thejns.org/view/journals/j-neurosurg/88/2/article-p243.xml.
35. Beck J, Ulrich CT, Fung C, Fichtner J, Seidel K, Fiechter M, et al. Diskogenic microspurs as a major cause of intractable spontaneous intracranial hypotension. Neurology. 2016;87(12):1220–6. http://www.ncbi.nlm.nih.gov/pubmed/27566748.
36. Brinjikji W, Savastano LE, Atkinson JLD, Garza I, Farb R, Cutsforth-Gregory JK. A novel endovascular therapy for CSF hypotension secondary to CSF-venous fistulas. AJNR Am J Neuroradiol. 2021;42(5):882–7. http://www.ncbi.nlm.nih.gov/pubmed/33541895.
37. Amrhein TJ, Williams JW, Gray L, Malinzak MD, Cantrell S, Deline CR, et al. Efficacy of epidural blood patching or surgery in spontaneous intracranial hypotension: a systematic review and evidence map. Am J Neuroradiol. 2023;44(6):730–9.
38. Langner S, Fleck S, Baldauf J, et al. Diagnosis and differential diagnosis of hydrocephalus in adults. Fortschr Rontgenstr. 2017;189:728–39.
39. Maller VV, Gray RI. Noncommunicating hydrocephalus. Semin Ultrasound CT MRI. 2016;37:109–19.
40. Kartal MG, Algin O. Evaluation of hydrocephalus and other cerebrospinal fluid disorders with MRI: an update. Insights Imaging. 2014;5:531–41.
41. Rovira A. Communicating hydrocephalus. Normal pressure hydrocephalus. In: Barkhof F, et al., editors. Clinical neuroradiology. Springer Nature Switzerland AG; 2019.
42. Ucar M, Guryildirim M, Tokgoz N, et al. Evaluation of aqueductal patency in patients with hydrocephalus: three-dimensional high-sampling-efficiency technique (SPACE) versus two-dimensional turbo spin echo at 3 Tesla. Korean J Radiol. 2014;15:827–35.
43. Bladowska J, Sasiadek MJ. Obstructive hydrocephalus in adults. In: Barkhof F, et al., editors. Clinical neuroradiology. Springer Nature Switzerland AG; 2019.
44. Barkovich AJ, Newton TH. MR of aqueductal stenosis: evidence of a broad spectrum of tectal distortion. Am J Neuroradiol AJNR. 1989;10:471–6.
45. Hodel J, Rahmouni A, Zins M, et al. Magnetic resonance imaging of noncommunicating hydrocephalus. World Neurosurg. 2013;79(2S):S21.e9–S21.e12.
46. Agarwal A, Bathla G, Kanekar S. Imaging of communicating hydrocephalus. Semin Ultrasound CT MR. 2016;37:100–8.
47. Shinoda N, Hirai O, Hori S, et al. Utility of MRI-based disproportionately enlarged subarachnoid space hydrocephalus scoring for

predicting prognosis after surgery for idiopathic normal pressure hydrocephalus: clinical research. J Neurosurg. 2017;127:1436–42.
48. Ishii K, Kanda T, Harada A, et al. Clinical impact of the callosal angle in the diagnosis of idiopathic normal pressure hydrocephalus. Eur Radiol. 2008;18:2678–83.
49. Virhammar J, Laurell K, Cesarini KG, Larsson EM. Preoperative prognostic value of MRI findings in 108 patients with idiopathic normal pressure hydrocephalus. AJNR Am J Neuroradiol. 2014a;35:2311–8.
50. Williams MA, Malm J. Diagnosis and treatment of idiopathic normal pressure hydrocephalus. Continuum (Minneap Minn). 2016;22(2 Dementia):579–99.
51. Nakajima M, Yamada S, Miyajima M, et al. Guidelines for management of idiopathic normal pressure hydrocephalus (third edition): endorsed by the Japanese Society of Normal Pressure Hydrocephalus. Neurol Med Chir (Tokyo). 2021;61:63–97.
52. Rovira À, Hodel J. Commentary: predictor of shunt response in idiopathic normal pressure hydrocephalus. Neuroradiology. 2022;64:2097–9.
53. Virhammar J, Laurell K, Cesarini KG, Larsson EM. The callosal angle measured on MRI as a predictor of outcome in idiopathic normal-pressure hydrocephalus. J Neurosurg. 2014b;120:178–84.